(Received 24 December 2024, Accepted 10 January 2025, Scheduled 21 January 2025)

# Reconfigurable Designs of Sectoral Microstrip Antennas for Single band and Tunable Circular Polarized Response

Amit A. Deshmukh*, Heet Mistry, Venkata A. P. Chavali, Aniruddh Viswanathan, and Prasanna Nadkarni

*EXTC, SVKM's DJSCE, Mumbai, India*

**ABSTRACT:** The circularly polarized design of a 350° sectoral microstrip antenna is proposed. Orthogonal surface current components at $TM_{10}$ mode on the sectoral patch provide circularly polarized characteristics. With the substrate thickness of $0.087\lambda_{cAR}$, it yields the simulated axial ratio bandwidth of 18 MHz (1.9%) that lies inside the reflection coefficient bandwidth of 487 MHz (44.66%). A reduction in the substrate thickness by $0.012\lambda_{cAR}$ in the 350° sectoral design is achieved by employing an H-shape ground plane profile. This design yields the axial ratio bandwidth of 13 MHz (1.45%), which is present inside the reflection coefficient bandwidth of 386 MHz (36.9%). The antenna using modified ground plane offers peak broadside gain of larger than 6 dBi. On conventional and H-shape ground plane design, the reconfigurable design of 350° sectoral patch is presented that offers switching between the wideband and circularly polarized characteristics. For operation at $TM_{30}$ mode in the Sectoral patch, circularly polarized reconfigurable configuration for sectoral angle decreasing from 340° to 280° is presented. Over this angle variation, the antenna offers tuning in the center frequency of axial ratio bandwidth by 367 MHz (20.6%) with a broadside gain of larger than 5 dBi. A design methodology for circularly polarized antennas functioning at $TM_{10}$ and $TM_{30}$ modes is proposed. It helps in realizing similar configuration as per specific wireless application. Experimental verifications for all the obtained results are carried out which show close agreement with the simulated results.

## 1. INTRODUCTION

Microstrip antenna (MSA) finds many applications in wireless communication, owing to its numerous advantages like low profile and planar configuration [1, 2]. In wireless communication, transmitted signal undergoes the effects of multi-path propagation, which leads to the changes in the direction of polarization of the incident wave. If this direction does not match with the receiver antenna polarization, a signal loss is observed. To overcome this, a circularly polarized (CP) antenna is selected. An important design feature of the MSA is the ease of generation of CP response, while employing simple modifications in the radiating patch [1, 2]. The CP response is obtained either by cutting a slot in the radiating geometry [3–5], or by placing a shorting post [6, 7], or by employing a modified shape of the radiating patch [8–10], or by cutting resonant slots inside the MSA [11–15], or by employing a modified ground plane structure in the form of slots or fractal shape geometries [16–19], or by adding parasitic patches in the planar or stacked layer [5, 20–22]. The CP MSAs obtained using slots and shorting post offer lower axial ratio (AR) bandwidth (BW) as they are fabricated on a thinner substrate. Modified patch shape geometries offering CP response either have lower AR BW due to the thinner substrate or employ complex shape of the radiating patch which increases the design complexity. CP designs using resonant slots are the optimum configurations since they offer 3–6% of AR BW, broadside gain greater than 6–8 dBi, and substrate thickness of $\geq 0.06\lambda_{cAR}$. In resonant slot cut designs, the appropriate knowledge of resonant modes on the patch is needed for placement of the slot. Also tuning in slot lengths does not yield tuning in the center frequency of AR BW, thus not able to cater wider frequency spectrum. A wideband CP design is needed when multiple wireless applications occupying nearby frequency bands are to be catered using a single antenna. A wideband CP design offering AR BW greater than 15% is obtained either by employing modified patch shape [23, 24] or modified resonant slot cut design [25] or by employing parasitic resonators [26–28]. These designs do offer higher AR BW but show variation in the broadside gain by 3 dBi. The frequency reconfigurable design using active elements discussed in [29] provides multi-band CP response, but tuning in those frequency bands is not possible. By incorporating open circuit stubs, a frequency reconfigurable design providing more than 30% tuning in the AR BW center frequency is discussed in [3]. However, this design shows 6 dBi variation in the broadside gain over the AR BW tuning range. Also, the addition of multiple rectangular stubs placed on the four edges adds to the design complexity.

This paper initially presents a proximity fed design of 350° Sectoral MSA (S-MSA) for CP response. Without incorporating any of the CP techniques mentioned above, a single sectoral patch configuration yields CP characteristics due to the presence of orthogonal surface currents at the fundamental $TM_{10}$ mode. The 350° S-MSA on substrate thickness of $0.087\lambda_{cAR}$ yields simulated AR BW of 18 MHz (1.9%) which lies inside the reflection coefficient ($S_{11}$) BW of 487 MHz (44.66%). By incorporating suitable modifications in the sectoral patch, its reconfigurable design is proposed, which offers switching in between the CP to wideband linearly polarized characteris-

* Corresponding author: Amit A. Deshmukh (amitdeshmukh76@gmail.com).

tics. The reconfigurable CP design offers simulated AR BW of 22 MHz (2.46%), which is present inside the $S_{11}$ BW of 453 MHz (41.31%). Across the AR BW antenna offers a peak gain of 6.7 dBic. The corresponding wideband design offers an $S_{11}$ BW of 387 MHz (33.9%) with a broadside peak gain of 9 dBi. Reduction in the substrate thickness in 350° S-MSA is achieved by using an H-shape ground plane profile. Against the conventional ground plane design and for substrate thickness reduction of $0.012\lambda_{cAR}$, H-shape ground plane antenna offers a simulated AR BW of 13 MHz (1.45%), which is present inside $S_{11}$ BW of 386 MHz (36.9%). Across the AR BW, the antenna offers the peak gain of more than 5 dBic. Reconfigurable wideband counterpart using H-shape ground plane offers an $S_{11}$ BW of 349 MHz (31.38%) with a peak gain of more than 6 dBi. A reconfigurable design of S-MSA for sectoral angle reducing from 340° to 280° is proposed. The reduction in sectoral angle increases the $TM_{30}$ mode resonance frequency of sectoral patch that yields tunable CP characteristics. With decrease in angle from 340° to 280°, center frequency of the AR BW increases from 1414 to 1781 MHz, thereby providing 367 MHz (20.6%) of frequency tuning. Across the complete range, the S-MSA operating at $TM_{30}$ mode provides a broadside gain of larger than 5 dBic. The design methodology to realize CP response in 350° S-MSA around the specific center frequency of the AR BW and tunable CP response in 340°–280° S-MSAs to cover specific wireless application spectrum is presented, which yields similar results. Thus, 350° S-MSA will help to cater to specific wireless application centered around the given frequency, and tunable CP antenna will cater to a complete range up to 20%. Without using the techniques of slot, stub, resonant slot, and by changing one of the patch parameters, tunable CP response is achieved in the present design. The novelty in the proposed work against the reported configuration is presented ahead in the paper. It shows that in terms of technique employed in the proposed design, against the tunable AR BW and gain achieved, the proposed designs offer optimum performance. The MSAs presented in this paper were initially optimized using CST simulations employing time domain solver [31], followed by the experimental verifications inside the Antenna laboratory, using instruments namely, ZVH-8, SMB 100A, and FSC 6. In all the designs, a close agreement is obtained between the simulated and measured results.

## 2. RECONFIGURABLE 350° S-MSA FOR CP RESPONSE

The S-MSA is a variation of circular MSA, and the wideband design of S-MSA against varying sectoral angle '$\theta$' has been reported in the literature [35]. In these designs, towards the band start frequencies of the $S_{11}$ BW; because of the orthogonal surface current variation at the fundamental mode on the patch, cross-polar radiation is higher [35]. To suppress this modal contribution, a shorted and slot cut wideband design of S-MSA is discussed in [36]. However, with the two shorting edges, this antenna offers maximum of the radiation pattern in the direction away from the broadside one, with a higher cross-polar radiation level. A circularly polarized design of shorted S-MSA employing a rectangular slot is discussed in [37]. With a shorting edge and slot contributing to the AR BW, the radiation pattern is tilted from the broadside direction. In this paper, without employing additional slot or shorting post, but by observing the modal current distribution at the fundamental mode on the sectoral patch against the sectoral angle, a CP design is presented as shown in Figs. 1(a) and (b). The sectoral patch of angle '$\theta$' is excited using the proximity feed as mentioned in the figure. The S-MSA is fabricated on an FR4 substrate ($\varepsilon_r = 4.3$, $h = 0.16$ cm), which is suspended above the ground plane using an air gap of $h_a$ cm. The air-suspended substrate configuration improves the antenna efficiency, while using a low cost lossy substrate. Also, it provides the reliability in the antenna results against the substrate parameter variations. For $h_a = 2.3$ cm, initially equivalent circular patch radius is selected such that its fundamental $TM_{11}$ mode frequency is around 1100 MHz. The radius '$r$' is found to be 5.5 cm. For this patch radius, various angle S-MSAs are realized as shown in Fig. 1(a). The parametric variations are carried out to study the excitation of resonant modes. Corresponding AR value variation resonance curve and AR plots for the same are shown in Figs. 1(c)–(f).

For the proximity feed at $x_f = 2.7$ cm and total substrate thickness of 2.46 cm, for each sectoral angle, two resonant modes are observed in the resonance curve. The surface current distributions were studied at the two peaks for every angle and are shown in Figs. 1(c), (d) for $\theta = 350°$. At the first mode, surface currents show one half wavelength variation along the patch perimeter. With this distribution, resonant mode is referred to as $TM_{10}$. In the sectoral geometry, fields will vary along two orthogonal dimensions of the patch, i.e., patch perimeter and radius. Thus in the modal identification, the first index refers to the number of half wavelength variations along patch perimeter, and the second refers to the number of half wavelength variation along radius. The second peak is due to $TM_{20}$ mode as two half wavelength variations are present along patch perimeter. This mode is similar to the $TM_{11}$ mode in circular patch. At $TM_{10}$ mode, the nature of surface currents variation leads to the orthogonal components over the patch. This yields CP radiation from the sectoral patch as visible from the AR plots, where for higher angles, AR value is close to 3 dBi. With the decrease in sectoral angle, this current orthogonality is not maintained which increases the AR value near the $TM_{10}$ mode frequency. The AR $\leq$ 3 dB is obtained for $\theta = 355°$, but an input impedance at the same is lower. This does not yield $S_{11}$ BW for $\leq -10$ dB. Against the feed point variation, an impedance matching for 355° S-MSA is achieved, but AR BW is not realized. As noted from the resonance curve plot shown in Fig. 1(e), impedance is higher at $TM_{10}$ mode for 350° S-MSA, but the AR value is more than 3 dB. The AR BW optimization for $\theta = 350°$ S-MSA is obtained by increasing the total substrate thickness to 2.86 cm ($h_a = 2.7$ cm). An increase in substrate thickness achieves equal amplitudes of the orthogonal currents on the patch to realize AR $\leq$ 3 dB and impedance matching for $S_{11} \leq -10$ dB. This design achieves simulated AR BW of 18 MHz (1.9%) that lies inside the $S_{11}$ BW of 487 MHz (44.66%). The total substrate thickness in terms of the wavelength at the center frequency of AR BW is $0.087\lambda_{cAR}$.

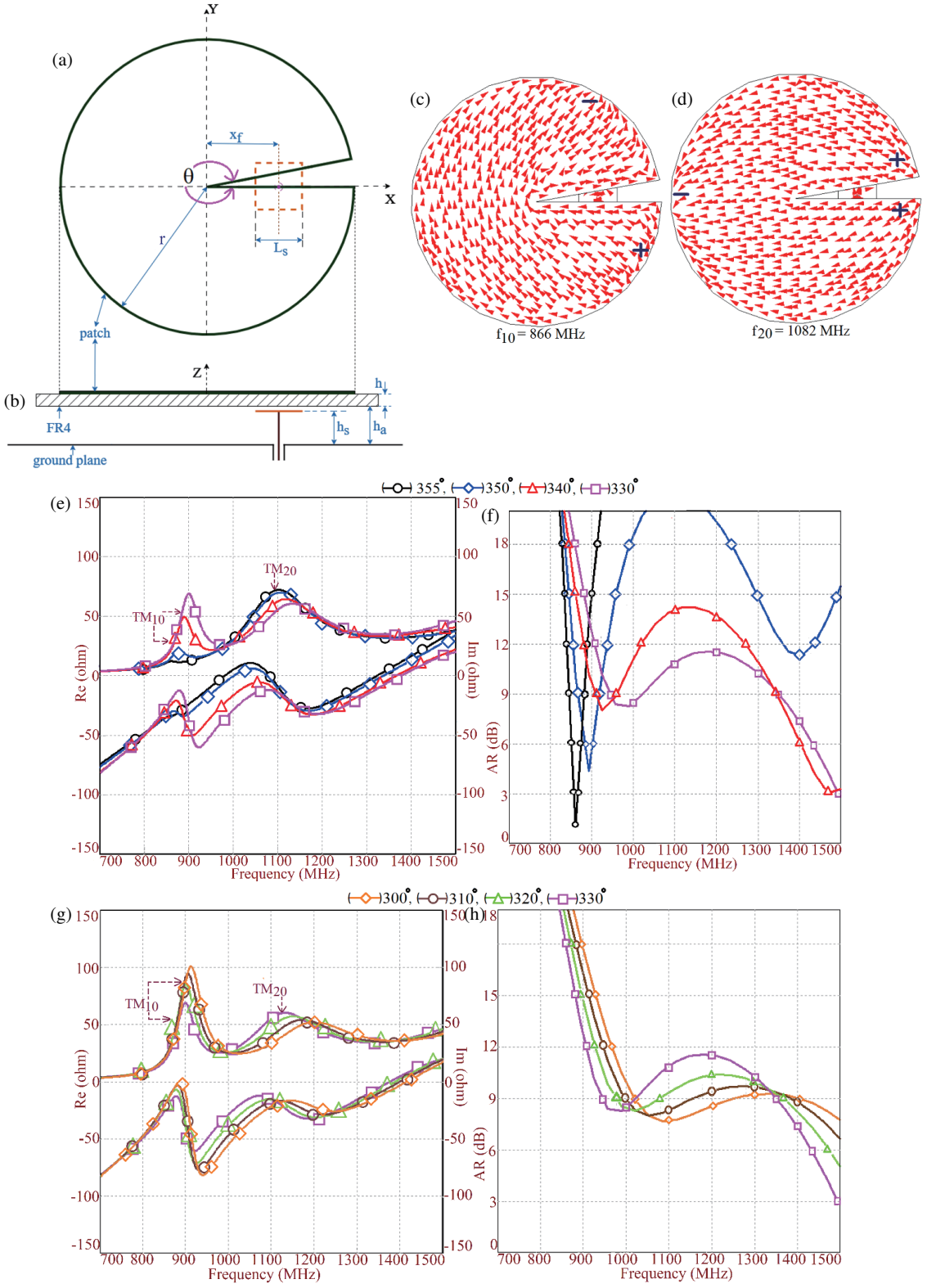


**FIGURE 1**. (a), (b) Proximity fed S-MSA, its (c), (d) surface current distribution at first two modes and (e)–(h) resonance curve and AR plots for varying Sectoral angle $\theta$.

The S-MSA is a variation of circular MSA (CMSA). Proximity fed CMSA for the same substrate thickness will realize wideband linearly polarized response. To obtain both the responses together using a single patch, a reconfigurable design of 350° S-MSA is proposed as shown in Fig. 2(a). To obtain a complete circular patch from 350° S-MSA, a small section of sectoral patch is placed inside the narrow slit in 350° S-MSA, as shown in Fig. 2(a). A small sectoral portion is connected to

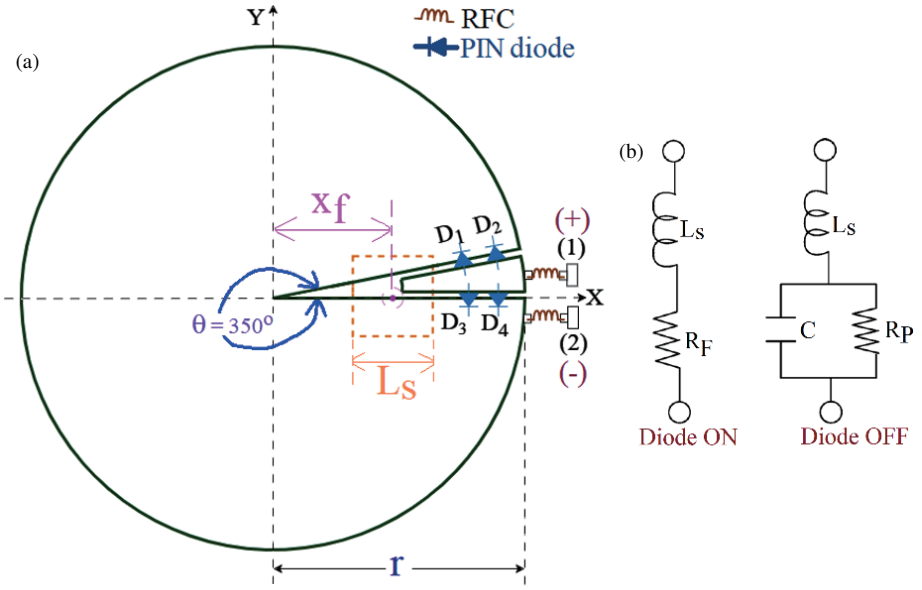


**FIGURE 2**. (a) Reconfigurable design of 350° S-MSA for CP and linear polarized wideband response, (b) equivalent circuit for PIN diode in ON and OFF state.

the 350° S-MSA through the activation of PIN diodes D1–D4. PIN diode BAR64-06W H6327 is selected. These diodes are provided with the DC biasing supply using biasing pads (1) & (2) and by using the series connection of RFC, ELT-3KN131B. The equivalent circuit of PIN diode is provided in Fig. 2(b). At the antenna operating frequency, when diode is ON, it offers forward resistance ($r_F$) of 3.4 Ω, which is a very small value. When diode is in OFF state, capacitor C and parallel resistance $r_P$ values are 0.25 pF and 3.2 kΩ, respectively. The $L_s$ equals 1.4 nH. Thus, when the diodes are OFF, i.e., no DC supply is connected to points (1) & (2), sectoral patch is disconnected from 350° S-MSA, and the antenna functions as a circularly polarized design. When diodes are forward biased by applying '+' polarity at (1) and '−' at (2), the small sectoral patch is connected to 350° S-MSA, and a complete circular configuration is obtained. This gives wideband linearly polarized response. The optimized reconfigurable design is achieved for the antenna parameters as, $h_a = 2.7$, $h = 0.16$, $h_s = 2.5$, $L_s = 1.7$, $x_f = 2.7$, $r = 5.5$ cm.

The results for the reconfigurable design in CP and wideband response are shown in Figs. 3(a)–(g) & 4(a)–(e). In the CP configuration, simulated and measured $S_{11}$ BWs are 453 MHz (41.31%) and 459 MHz (42.05%), respectively as shown in Fig. 3(c). The AR BWs observed in the simulation and measurement are 22 MHz (2.46%) and 25 MHz (2.8%), respectively. Across the AR BW, peak antenna gain is more than 6 dBic. Radiation pattern plots shown in Figs. 3(e), (f), at the center frequency of AR BW, are in the broadside direction with a higher cross polar level of radiation. The higher cross-polar levels are attributed to the presence of CP radiation from the antenna. With respect to time and the observer, current vectors rotate in clockwise direction. But with respect to antenna they will show anticlockwise rotation, thereby giving left hand CP (LHCP) response as shown in Figs. 3(g) & 4(a)–(d). Using conversion equations and vertical, linear polarization $E$-field components obtained in the pattern measurement, LHCP and right hand CP (RHCP) components are practically evaluated [34], which shows close agreement against the simulations. The fabricated antenna setup is shown in Figs. 3(a), (b).

In the broadband design, i.e., when the diodes are forward biased, the $S_{11}$ BWs observed in the simulation and measurement are 387 MHz (33.9%) and 386 MHz (34.06%), respectively as shown in Fig. 3(d). The antenna offers broadside radiation pattern across the $S_{11}$ BW with E-plane aligned along $\Phi = 0°$. The peak antenna gain is close to 9 dBi. Radiation pattern, AR BW, and gain were measured inside the antenna laboratory as shown in Fig. 4(e). In this, far-field distance calculated with respect to the highest frequency of $S_{11}$ BW was maintained between the reference Horn antenna and antenna under test (AUT). For all the measurements in this paper, far-field distance of 300 cm was maintained between the two antennas. Around the measurement desk, reflecting metallic objects were not present. The distance of adjoining walls from the central measurement desk is more than six times of the wavelength, calculated with respect to the lowest frequency of measurement. All these details ensure minimum reflection environment and as close as possible to the ideal anechoic chamber measurements. The broadside antenna gain was measured using three-antenna method for a better accuracy.

Substrate thickness in the reconfigurable circularly polarized 350° S-MSA is 2.86 cm, i.e., $0.087\lambda_{cAR}$. This value is calculated with respect to the wavelength ($\lambda_{cAR}$) at the center frequency of AR BW. The reduction in substrate thickness is achieved by employing an H-shape ground plane profile, as shown in Figs. 5(a), (b). In this design, a three-layer suspended configuration is selected in which two layers of FR4 substrate are separated by an air gap of $h_a$ cm. The optimization procedure of H-shape ground plane for wideband and CP

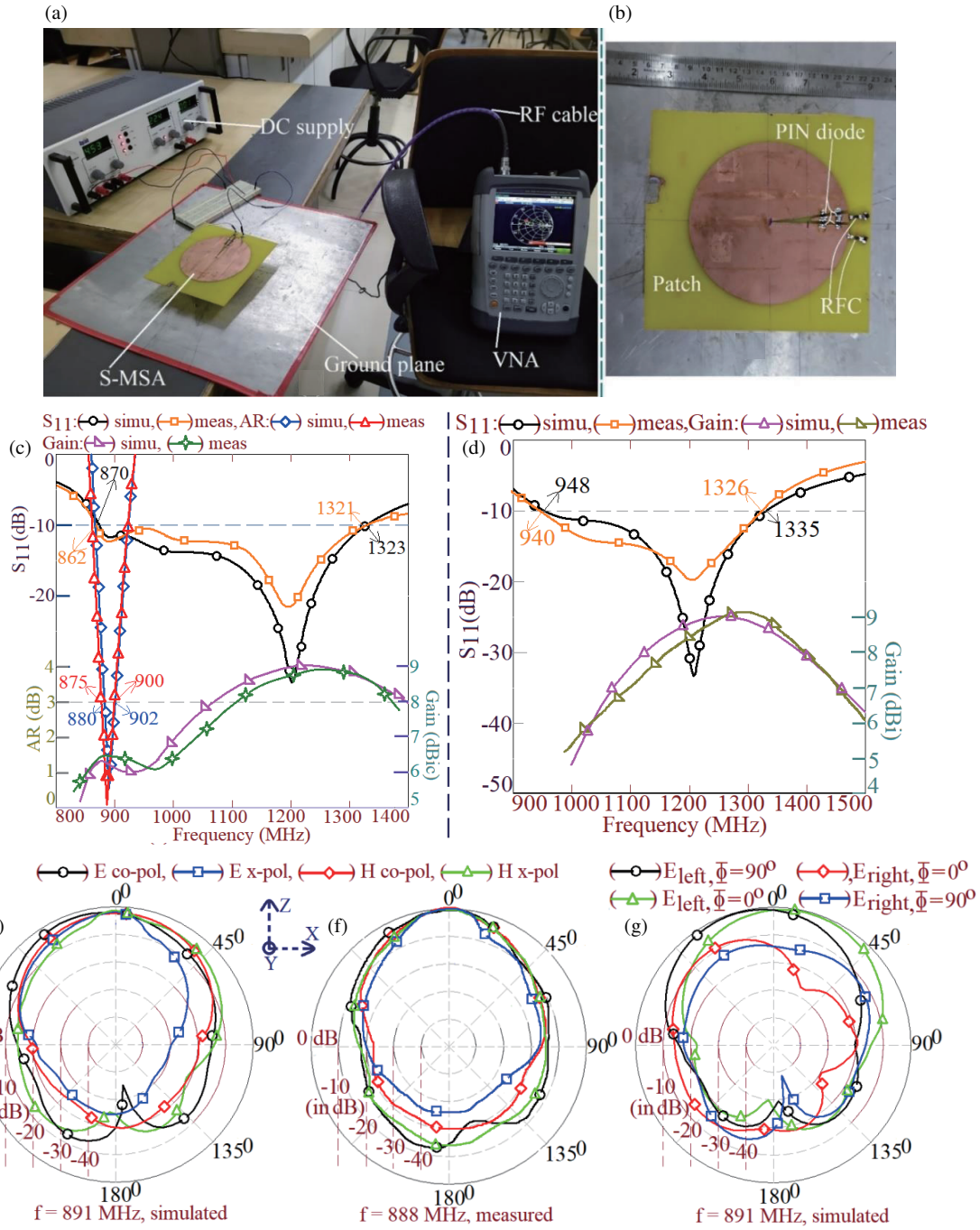


**FIGURE 3**. (a) $S_{11}$ BW measurement setup, (b) fabricated antenna, optimum results for (c) CP and (d) wideband design and (e), (f) radiation pattern and (g) simulated field polarization plots for reconfigurable design of 350° S-MSA for CP response.

designs is discussed in [38] and hence not presented here. Using modified ground plane, antenna gain decreases. Hence, there exists a trade-off between the substrate thickness reduction achieved against decrement in the gain [38]. Optimum design is considered the one that provides a peak gain of more than 6 dBi. This value is selected since it is an appreciably large gain from the practical applications. As per this condition, optimum design using H-shape ground plane profile is obtained for $h_a = 2.2$ cm, i.e., for the total substrate thickness of 2.52 cm, with all the other sectoral patch parameters remaining unchanged. Results for this design are shown in Figs. 5 & 6.

In the broadband design using H-shape ground plane, the $S_{11}$ BWs observed in the simulation and measurement are 349 MHz (31.48%) and 367 MHz (33.01%), respectively. The antenna offers broadside radiation pattern with E-plane aligned along $\Phi = 0°$ and peak antenna gain of more than 6 dBi. In the circularly polarized configuration, simulated and measured $S_{11}$ BWs are 386 MHz (36.9%) and 391 MHz (37.61%), respectively. The AR BWs observed in the simulation and measurement are

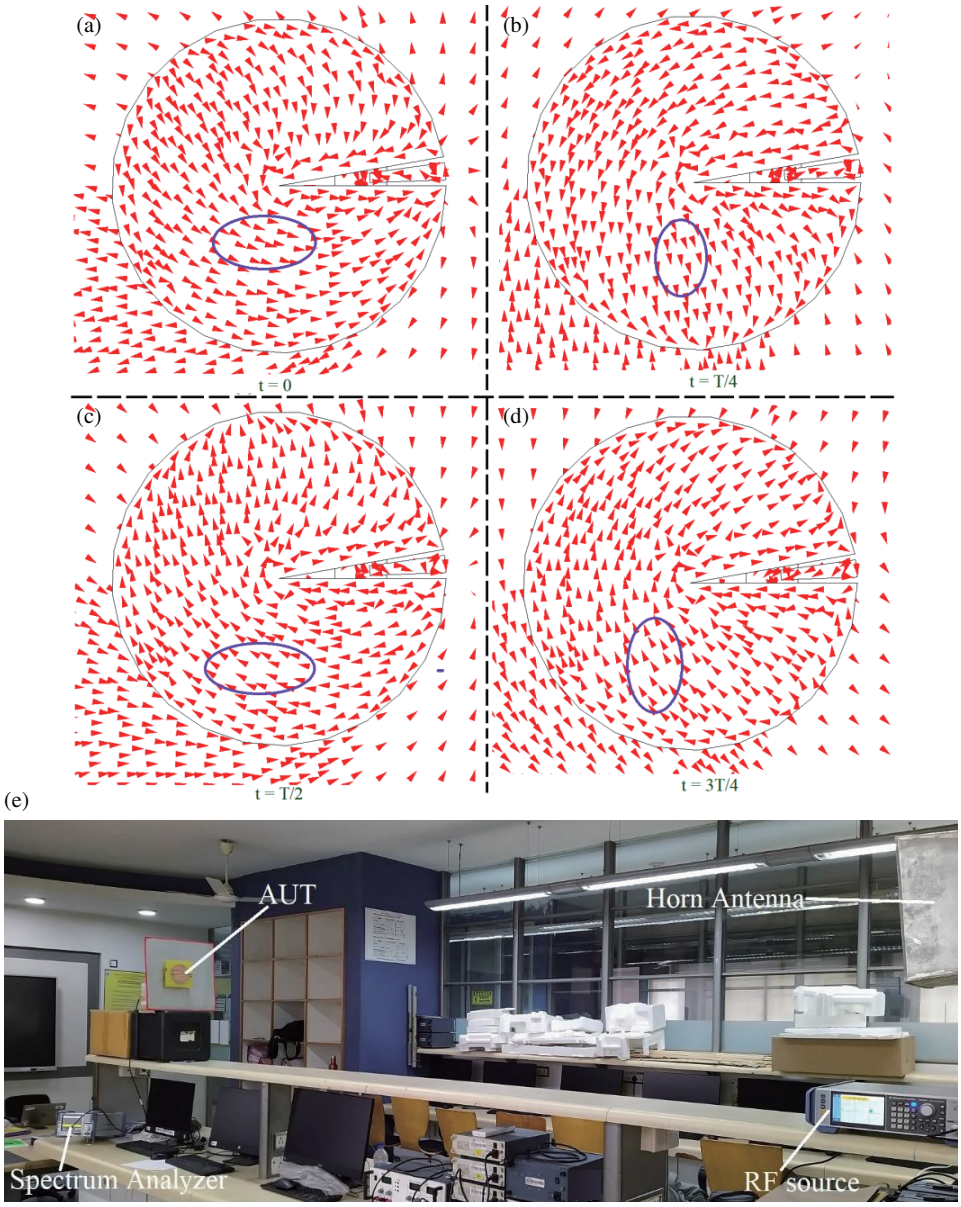


**FIGURE 4**. (a)–(d) Time varying surface current distribution at the center frequency of AR BW and (e) gain measurement setup for reconfigurable design of 350° S-MSA for CP and wideband response.

13 MHz (1.45%) and 18 MHz (2.02%), respectively. Across the AR BW, peak antenna gain is more than 6 dBic. The radiation pattern at the center frequency of AR BW is shown in Figs. 6(a)–(c). The pattern remains in the broadside direction with a higher cross-polar component. The antenna offers LHCP response over the AR BW. The measured right hand and left hand CP field components, calculated using the conversion equations applied to the measured values of horizontal and vertical polarization $E$-field values, agree closely with the simulation. With reference to the wavelength at the center frequency of AR BW, substrate thickness is $0.075\lambda_{cAR}$. In comparison with the conventional ground plane, H-shape ground plane design offers $0.012\lambda_{cAR}$ reduction in substrate thickness. It should be noted here that conventional ground plane used above was square with side length 35 cm, against a 15 cm square ground plane ($L_g = W_g$) employed in the H-shape ground plane profile. Using square ground plane of $L_g = 15$ cm, 350° sectoral patch does not offer CP response. But the same was achieved while realizing H-shape profile. Thus, although reduction in the substrate thickness is small, and AR BW is reduced by a small margin, H-shape ground plane profile provides a technique to achieve CP response in sectoral patch, while using a small ground plane size. The measurement setup for a small sized modified ground plane antenna is provided in Fig. 6(d).

## 3. RECONFIGURABLE FREQUENCY TUNABLE S-MSA FOR CP RESPONSE

In wireless applications frequency tuning of the AR BW center frequency is needed so as to cover many adjoining frequency

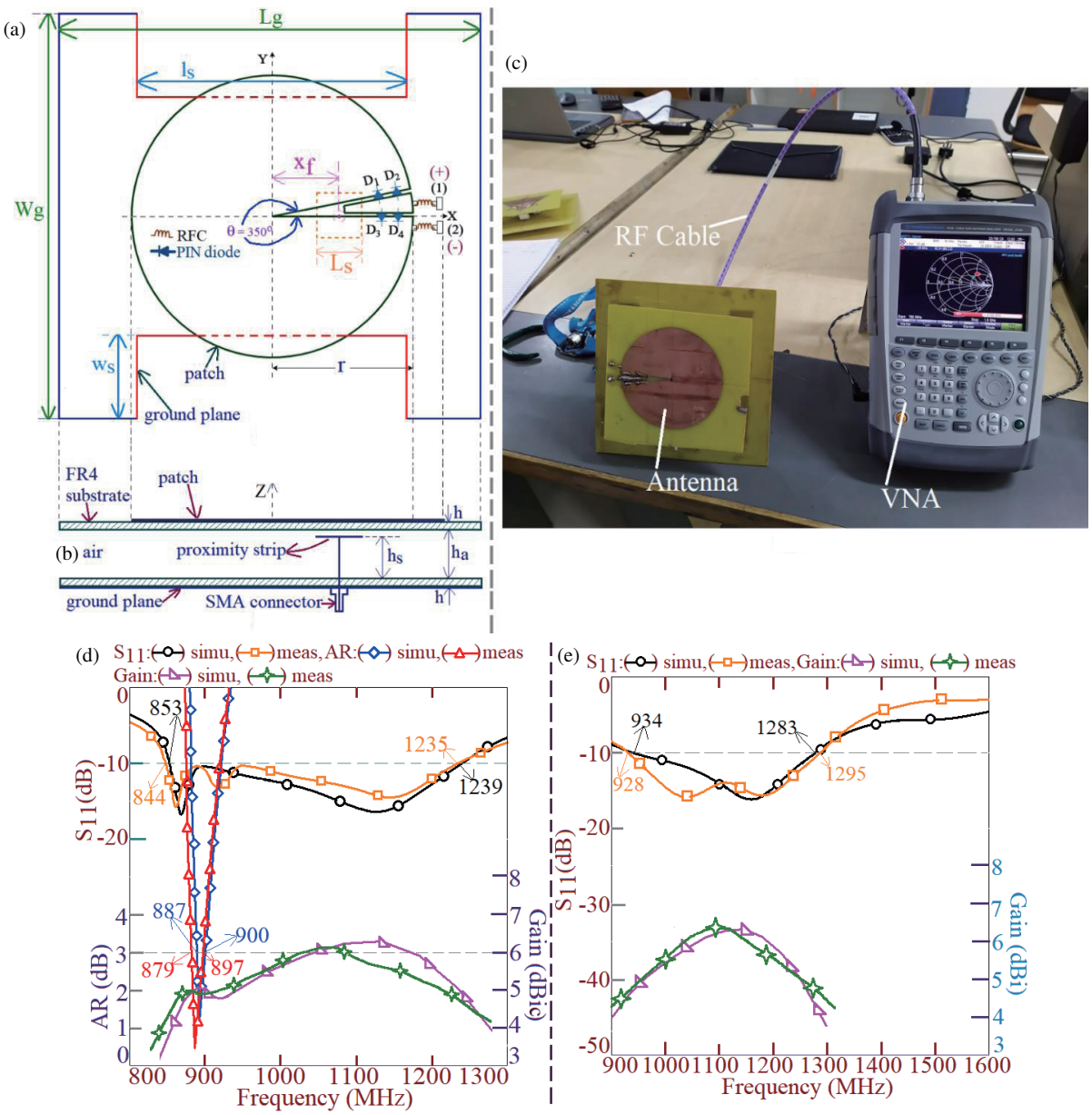


**FIGURE 5**. (a), (b) Reconfigurable 350° S-MSA backed by H-shape ground plane, its (c) $S_{11}$ BW measurement setup and optimum response for (d) CP and (e) wideband response.

spectrums. In the proposed single patch CP S-MSA, with the decrease in sectoral angle, AR BW is not achieved. In 350° S-MSA, tuning in the center frequency of AR BW will require changing the patch radius. Thus while operating at $TM_{10}$ mode in sectoral patch tuning in the AR BW center frequency cannot be obtained. In sectoral patch, next two resonant modes are $TM_{20}$ and $TM_{30}$, at which surface currents exhibit two and three half wavelength variations along the patch perimeter. With this distribution, the antenna offers broadside radiation pattern at two frequencies with E-plane aligned along $\Phi = 0°$. Further, as seen from the parametric study given in Figs. 1(e)–(h), AR value decreases towards the higher frequencies with the decrease in sectoral angle. This behavior of S-MSA is studied further for the possible tuning of AR BW center frequency against the sectoral angle. For $r = 5.5$, $h_a = 2.3$, $x_f = 2.7$ cm, parametric study is carried out, and resonance curve and AR plots for sectoral angle decreasing from 355° to 270° are shown in Figs. 7(a)–(f).

In the resonance curve, the first two resonant modes correspond to $TM_{10}$ and $TM_{20}$ as described earlier. The next resonant mode is $TM_{30}$. At this mode, surface currents exhibit three half wavelength variations in modal currents as mentioned in Fig. 8(a). Near this resonant mode frequency, AR value lower than 3 dB is observed. Similar to $TM_{10}$ mode, with three half wavelength variation in surface currents at $TM_{30}$ mode, orthogonality in current vectors is obtained over the sectoral patch that achieves CP response with AR value less than 3 dB. With the decrease in sectoral angle, perimeter length of the sectoral patch decreases which increases $TM_{30}$ mode frequency. With this CP response is obtained in higher frequency region

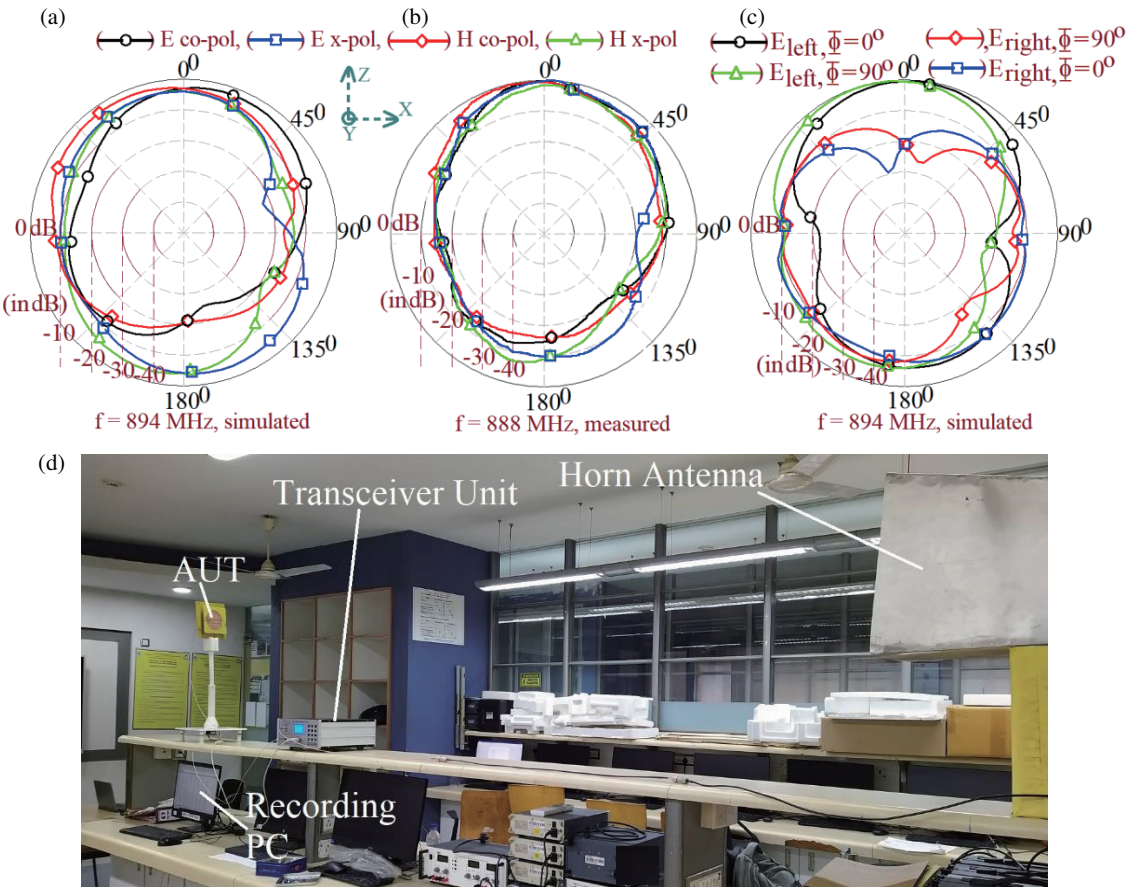


**FIGURE 6**. (a), (b) Radiation pattern and (c) simulated field polarization plots and (d) radiation pattern measurement setup for reconfigurable design of 350° S-MSA backed by H-shape ground plane.

as reflected in Fig. 7. For $\theta = 340°$, CP response is obtained around 1450 MHz, whereas for $\theta = 280°$, it is obtained around 1850 MHz. Thus, the reduction in sectoral angle by 60° yields tuning in the center frequency of AR BW by 400 MHz. To realize this varying angle sectoral patch so as to achieve frequency tuning, the reconfigurable design of S-MSA for angle decreasing from 340° to 280° is developed as shown in Fig. 8(b).

In the present case, a reconfigurable design that yields various S-MSAs for $\theta = 340°$, 320°, 300°, and 280° is proposed. A step of 20° is considered for achieving each of the reconfigurable S-MSAs. This step angle is a function of center frequency of the AR BW that needs to be tuned to for every angle $\theta$, and thus it can change as per specific wireless application. Initially, S-MSA of $\theta = 280°$ is selected for $r = 5.5$ cm. Further, radii $r_1$, $r_2$, $r_3$ of circular sectoral patches are selected as 5.0, 5.3, 5.5, respectively, whereas angle $\theta_1$ for each sector is taken as 18°. With this selection of sectoral angle and sectoral patch radius, the air gap of 0.1 cm is maintained between the individual patches at which PIN diodes D1–D12 are placed as shown in Fig. 8(b). Each narrow sectoral patch is connected with a biasing pad through RFC, for providing the DC supply. When all the diodes are forward biased with the polarities shown, all the sectoral patches and 280° S-MSA are inter-connected, which yields 340° S-MSA. When DC supply is provided at pads (1), (2), and (3) only, 320° S-MSA is realized, whereas with supply connected at pads (1) and (2), 300° S-MSA is obtained. When supply is not connected to any of the DC pads, 280° S-MSA is realized. For $h_a = 2.3$, $L_s = 1.4$, $x_f = 2.7$ cm, and with suitable excitation of PIN diodes, 340°–280° S-MSAs are obtained that achieves tuning in the center frequency of AR BW. The results for all the reconfigurable S-MSAs are tabulated in Table 1. The plots for 340° and 280° S-MSAs are provided in Figs. 9 and 10. In all the sectoral MSAs, the $S_{11}$ BW of more than 20% is achieved. With reference to the simulated AR BW, while going from 280° to 340° S-MSA, center frequency decreases from 1781 to 1414 MHz, thereby giving 367 MHz (20.6%) of frequency tuning. This frequency tuning range will help to cover most of the practical wireless applications using a single antenna. The peak antenna gain is 8.0 dBic for 340° S-MSA, whereas it is 5.9 dBic for 280° S-MSA. The reduction in peak antenna gain in smaller sectoral angle S-MSA is attributed to the higher contribution of vertical surface currents. In 280° and 340° S-MSAs, radiation pattern at the center frequency of AR BW is in the broadside direction with a higher cross-polar level. The simulated polarization plot shows the dominance of $E$-left hand fields, thus giving LHCP response. Measured left and right hand polarization $E$-fields are calculated using the vertical and horizontal polarization values as obtained in the pattern measurements [34]. The measured field polarization plot also confirms the presence of

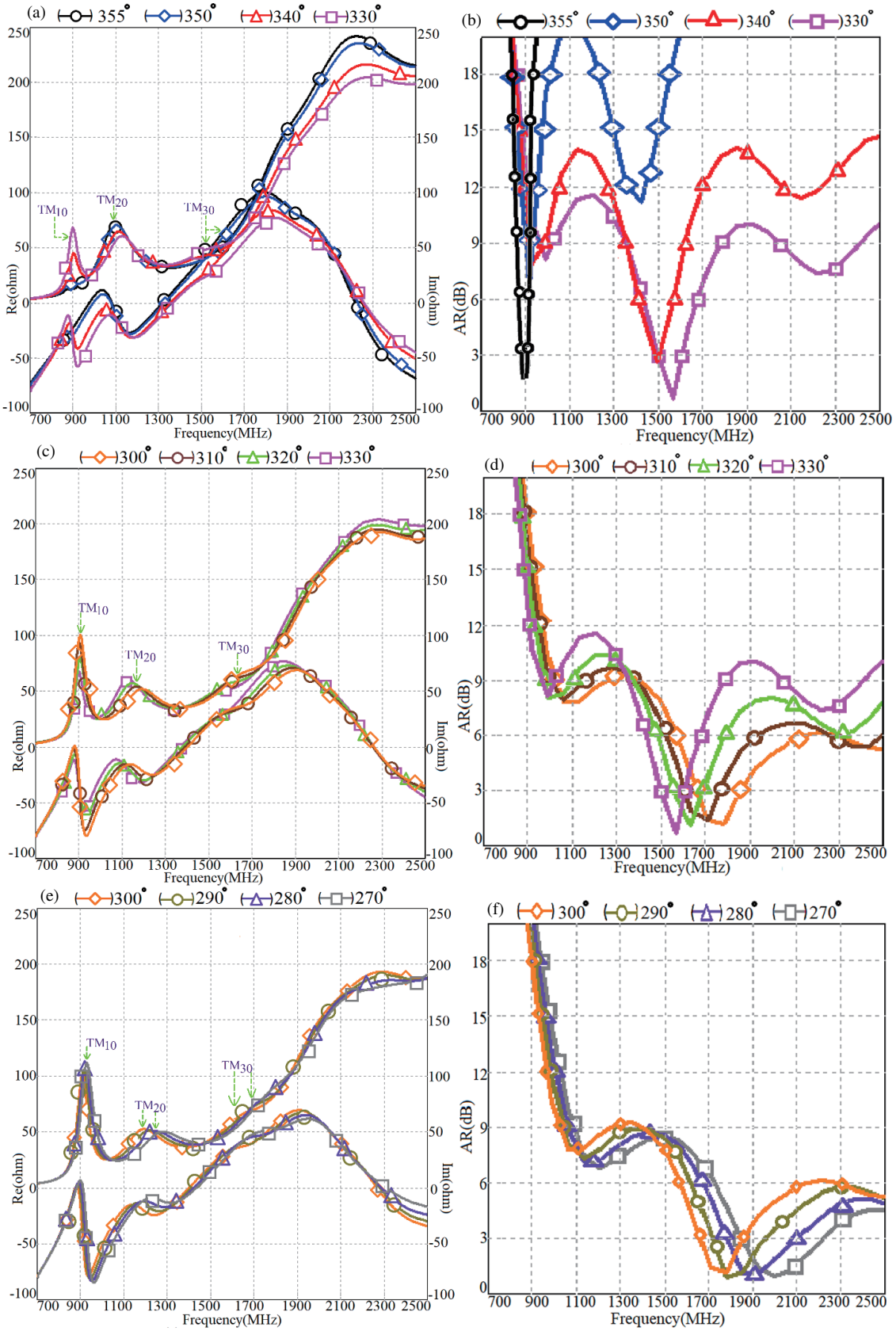


**FIGURE 7**. (a)–(f) Resonance curve and AR plots for S-MSA backed by conventional ground plane for decreasing Sectoral angle '$\theta$'.

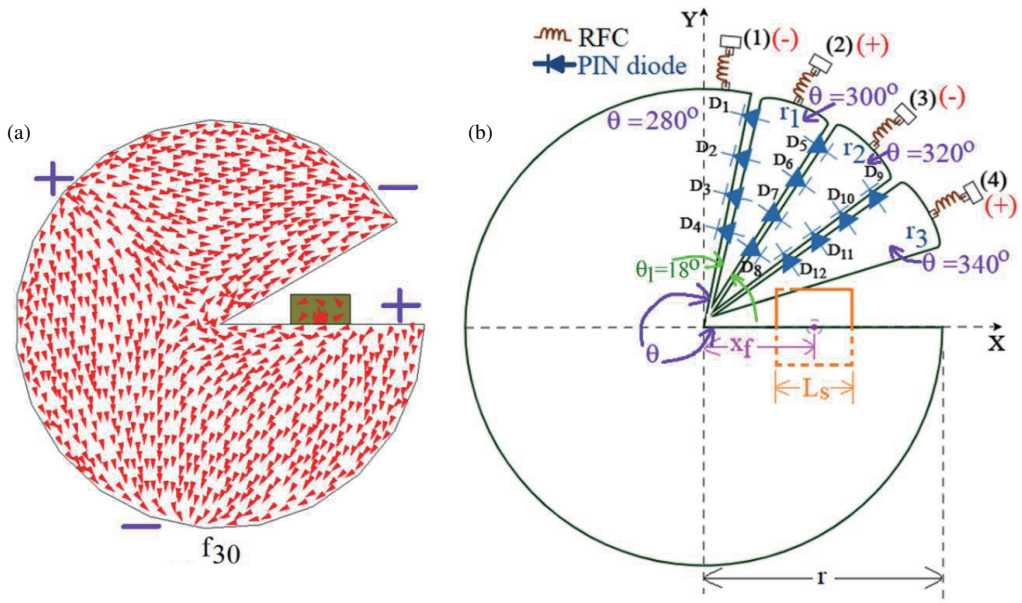


**FIGURE 8**. (a) Surface current distribution at $TM_{30}$ mode for S-MSA for $\theta = 330°$ and (b) reconfigurable design of S-MSA for $\theta$ reducing from 340° to 280°.

**TABLE 1**. Results for reconfigurable 280 to 340 S-MSAs.

| MSA | Simu. BW $S_{11} \leq -10$ dB (MHz, %) | Meas. BW $S_{11} \leq -10$ dB (MHz, %) | Simu. BW AR $< 3$ dB (MHz, %) | Meas. BW AR $\leq 3$ dB (MHz, %) | $f_{cAR}$ (MHz) | Peak Gain (dBic) |
|---|---|---|---|---|---|---|
| 340° S-MSA | 304, 20.29 | 323, 21.98 | 68, 4.8 | 72, 5.14 | 1414 | 8.0 |
| 320° S-MSA | 361, 23.72 | 378, 24.08 | 141, 9.2 | 145, 9.4 | 1532 | 6.5 |
| 300° S-MSA | 384, 24.12 | 395, 24.56 | 174, 10.31 | 181, 10.7 | 1687 | 6.2 |
| 280° S-MSA | 394, 23.67 | 403, 24.32 | 134, 7.52 | 132, 7.46 | 1781 | 5.9 |

LHCP radiation. Similar radiation pattern characteristics are obtained in 300° and 320° S-MSAs.

The simulated CST model for the reconfigurable antenna and orthogonal $E$-fields amplitude and phase plots generated using CST simulations for orthogonal probes placed in the far-field region, for all the reconfigurable S-MSAs are provided in Figs. 11 and 12.

In all the reconfigurable designs, near the respective AR BW range, $E_x$ and $E_y$ values are nearly equal. The phase component $\varphi_y$ either leads $\varphi_x$ by 90° or lags by 270° in all the designs. With respect to antenna as a radiator, this phase difference confirms the presence of LHCP radiation from the S-MSAs.

In the two S-MSAs, CP response is obtained around the fundamental $TM_{10}$ and third order $TM_{30}$ modes. Unlike the orthogonal resonant modes present in the generation of CP response, in the proposed design, only a single mode yields the CP characteristics. In the literature on slot cut MSA, an explanation can be found related to the presence of orthogonal mode currents on the patch that achieves the CP characteristics [12]. The CP characteristics are further proven with the help of time varying surface current distribution at a point on the patch [12]. A similar theory is drawn here to explain the CP response in S-MSA. The surface current distributions at $TM_{10}$ mode on 350° and 330° S-MSAs are shown in Figs. 13(a), (b). Resonant field/surface current follows one half wavelength variation along the patch perimeter length. The current and $E$-field magnitude plots at $TM_{10}$ mode from point A to B are provided in Fig. 13(c). Over the field/current variation length, for a phase point '$\theta$' around 45° along the respective waveforms, there exists an equal magnitude, opposite field polarity (same current amplitude) point on the waveform, which is spaced by phase difference of $\pi/2^c$, i.e. around 135°. As seen from the current direction plots for 350° S-MSA, these two equal magnitude field/current points lie on the directions J1 and J2 vectors, which are orthogonal to each other. On the sectoral patch there will be such a pair of points for these '$\theta$' combinations. This realizes equal magnitude current vector/$E$-field points, which are orthogonal in direction and separated by $\pi/2^c$ in phase. This condition of current vectors/$E$-field points on the sectoral patch for 350° S-MSA satisfies the CP radiation requirements. Against this, on 330° S-MSA, effective J1 and J2 current vectors are not orthogonal in direction, and thus even if magnitudes of pairs of current vectors are the same, they do not meet all the requirements for CP radiation. Hence at $TM_{10}$ mode, 350° S-MSA only gives CP characteristics. The time varying current distribution, shown in Figs. 4(a)–(d), confirms the CP findings.

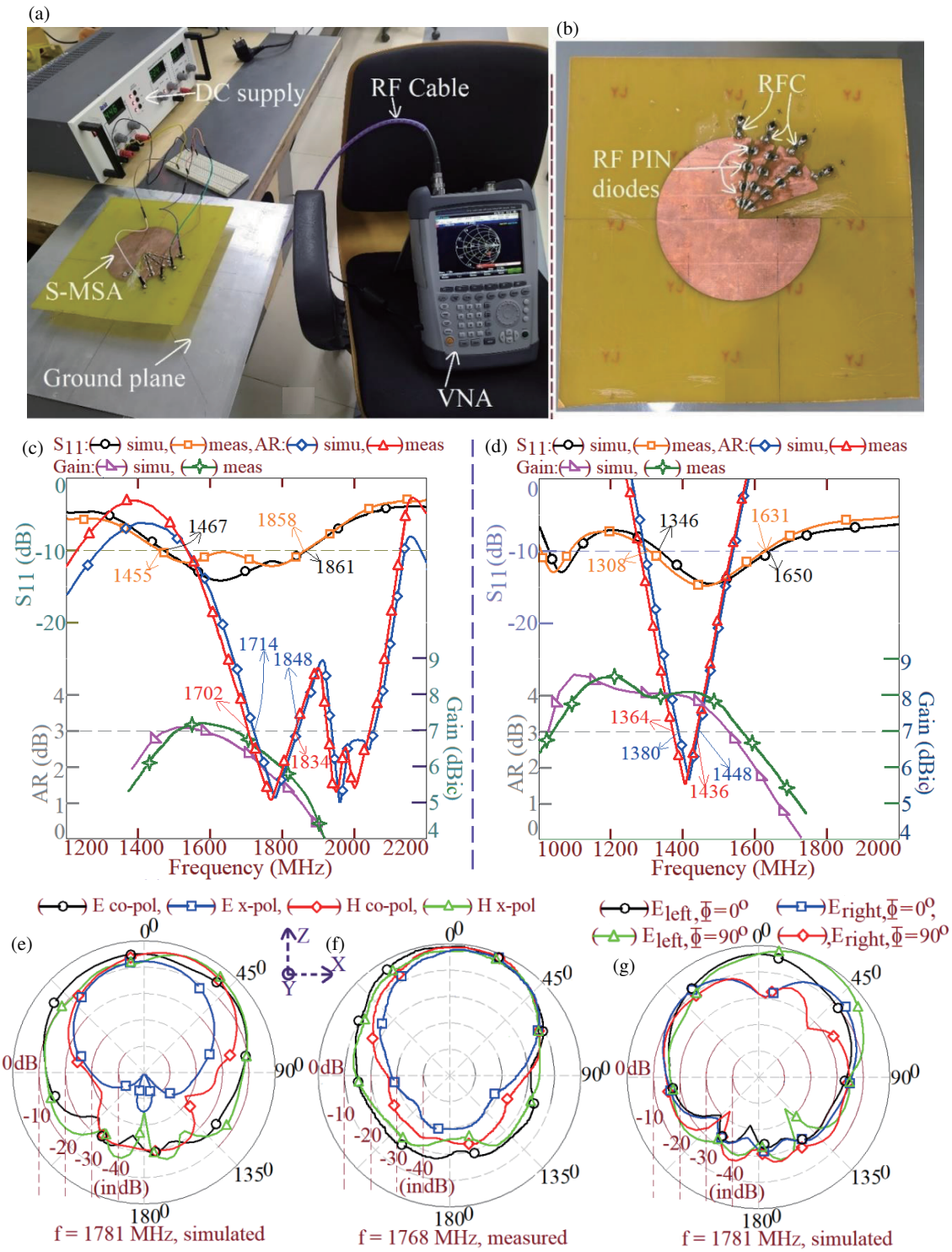


**FIGURE 9**. (a) $S_{11}$ BW measurement setup and (b) fabricated prototype for reconfigurable design of S-MSA for CP response around $TM_{30}$ mode, optimum response for reconfigurable (c) 280° and (d) 340° S-MSA, and (e), (f) radiation pattern and (g) simulated field polarization plots for 280° S-MSA.

Similar explanation is drawn at $TM_{30}$ resonant mode. Over the sectoral patch, three half wavelength variation in currents/$E$-field exists. For this effective surface current directions are J1, J2, and J3 as shown in Fig. 13(d). Based on these three current vectors, effective orthogonal current vectors Jx and Jy are derived. On these vector directions, a pair of points exists at which currents/fields are orthogonally placed in space on the sectoral patch, and at a phase angle of $\theta$ and $\theta + \pi/2^c$, with an equal magnitude, thus satisfying the requirements for the CP radiation. Thus similar to slot cut MSA, orthogonal current vectors provide CP response, on the sectoral patch.

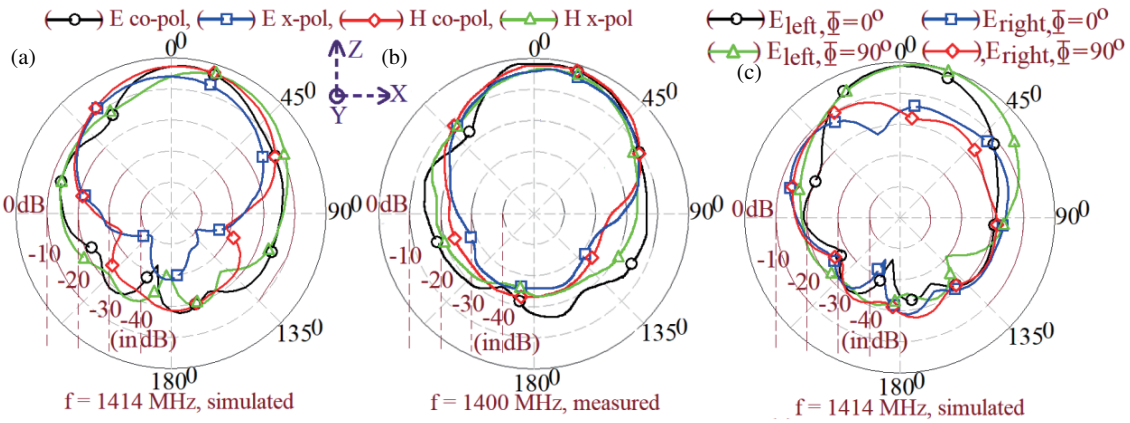


**FIGURE 10**. (a), (b) radiation pattern and (c) simulated field polarization plots for 340° S-MSA.

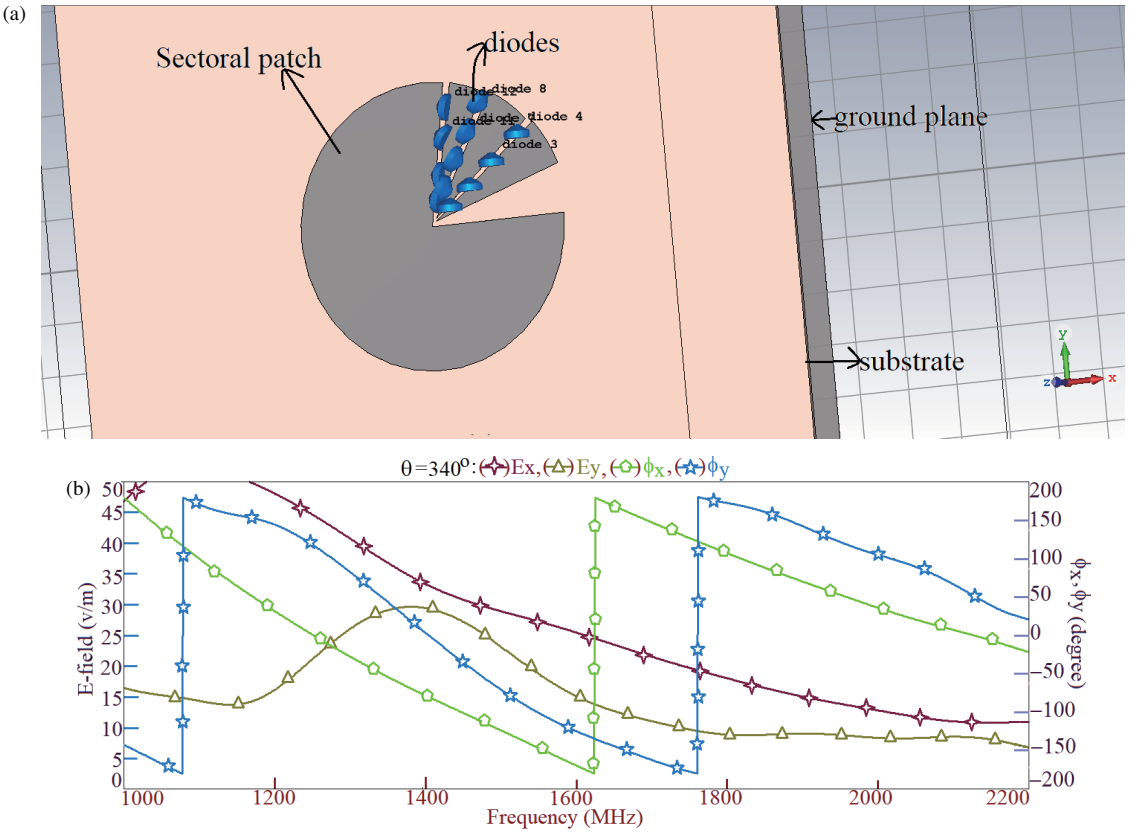


**FIGURE 11**. (a) CST mode for reconfigurable antenna, and (b) $E$-fields amplitude and phase plots for 340° S-MSAs.

## 4. DESIGN METHODOLOGY FOR 350° S-MSA AND RECONFIGURABLE S-MSAS

In 350° sectoral patch, resonant length at fundamental $TM_{10}$ mode is formulated by using Equation (1). To realize this equation, surface current paths at $TM_{10}$ mode are studied as shown in Fig. 13(a). While arriving at the equation, average of the two path lengths, 1 & 2, as mentioned in Fig. 13(a), is considered. As the currents along path 1 are not completely following the full perimeter length in the sector, weighting factor as mentioned in Equation (1) for path 1 contribution is considered. The resonance frequency at $TM_{10}$ mode is calculated by using Equation (2). An effective dielectric constant ($\varepsilon_{re}$) for the suspended substrate is calculated by using Equation (3). For the above patch parameters, calculated frequency using Equation (2) is 875 MHz that matches closely with the simulated value of 866 MHz.

$$L_{e10} = 2r\left(\left({}^{240}/_{360}\right)\pi + 1\right)\Big/_{2} \tag{1}$$

$$f_{10} = {}^{30}/_{2L_{e10}\sqrt{\varepsilon_{re}}} \tag{2}$$

$$\varepsilon_{re} = \frac{\varepsilon_r\left(h + h_a\right)}{h + h_a\varepsilon_r} \tag{3}$$

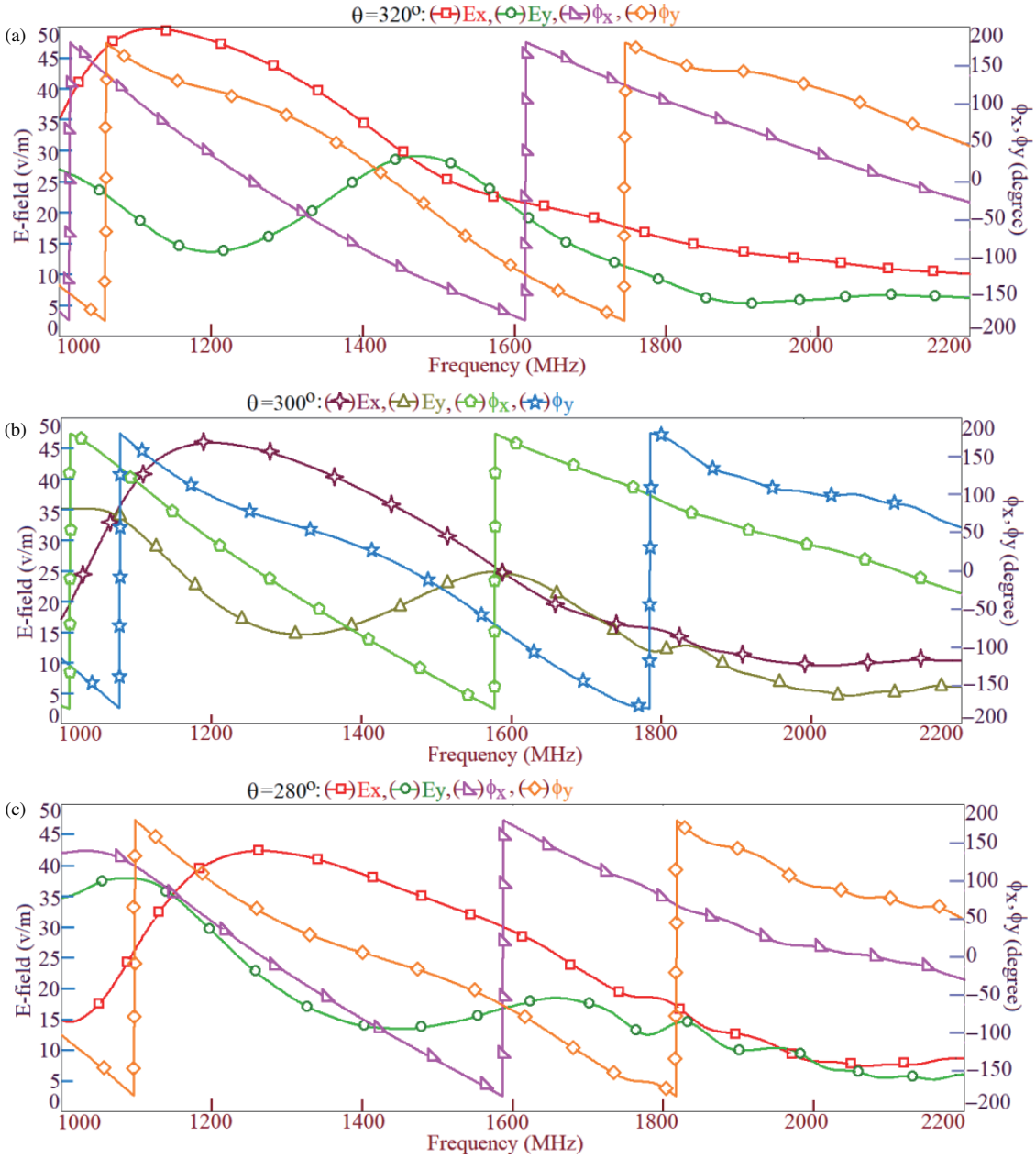


**FIGURE 12**. $E$-fields amplitude and phase plots for (a) 320°, (b) 300° and (b) 280° S-MSAs.

The design methodology for 350° S-MSA is initiated by specifying the center frequency of AR BW, $f_{cAR}$. The $TM_{10}$ mode frequency in 350° S-MSA is calculated by using this frequency as mentioned in (4). The substrate thickness for the patch is selected as given in Equation (5). The value of substrate thickness and the frequency relation between $f_{cAR}$ and $f_{10}$ are the same as that present in the original 350° S-MSA discussed above. At the new frequency $f_{10}$, as air gap thickness is not available, the value of $\varepsilon_{re}$ is unknown to begin with. Hence, an initial approximation of 1.055 is taken. This approximation is based on the value of $\varepsilon_{re}$ as present in the above optimum design. Using the calculated value of $h_t$ and for FR4 substrate, $h_a$ is selected, which is an integer and practically realizable number. Using these substrate parameters, $\varepsilon_{re}$ is recalculated using Equation (3), and it is retained in all further calculations. The resonant length at $TM_{10}$ mode in 350° S-MSA is calculated by using Equation (6), whereas patch radius is obtained using (7). Equation (7) is realized from Equation (1). The proximity strip parameters are calculated as $h_s = 0.0745\lambda_{10g}$, $L_s = 0.051\lambda_{10g}$, $x_f = 0.491r$. Here, $\lambda_{10g}$ is the wavelength at $TM_{10}$ mode in 350° S-MSA, as calculated using Equation (8). In all the equations discussed in this section, frequency is mentioned in GHz, and antenna dimension is calculated in cm. Using the above methodology, the 350° S-MSA is designed for $f_{cAR} = 1176$ MHz in the GPS L5 band. Various calculated antenna parameters are $h = 0.16$, $h_a = 2.1$, $r = 4.0$, $h_s = 1.9$, $L_s = 1.5$, $x_f = 2.0$ cm. This antenna offers simulated and measured $S_{11}$ BWs of 581 MHz (41.22%) and

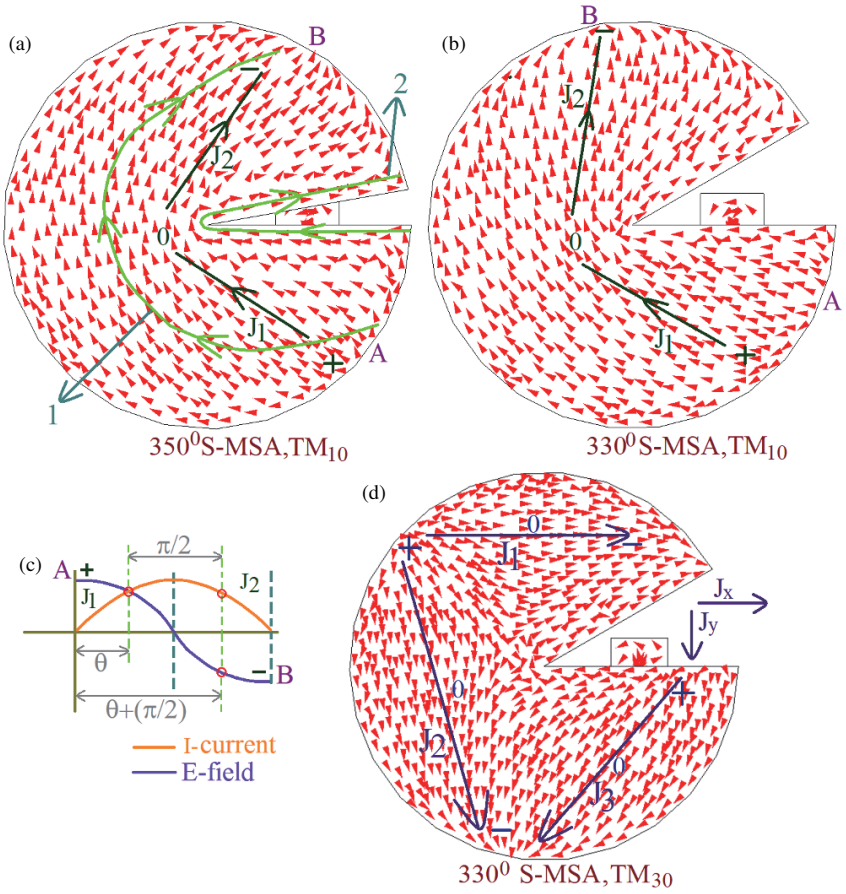


**FIGURE 13**. Surface current distribution at $TM_{10}$ mode in (a) 350° and (b) 330° S-MSA, (c) current and $E$-field plots on Sectoral patch, and (d) surface current distribution at $TM_{30}$ mode for 330° S-MSA.

599 MHz (42.03%), respectively. The AR BWs observed in the simulation and measurement are 24 MHz (2.08%) and 28 MHz (2.6%), respectively. Across the AR BW, the antenna offers a peak gain of 6 dBic. The center frequency of AR BW in the simulation is 1149 MHz, which is very close to the desired frequency of GPS L5 band.

$$f_{10} = {}^{f_{cAR}}/_{1.01} \tag{4}$$

$$h_t = 0.09\left({}^{30}/_{f_{10}\sqrt{\varepsilon_{re}}}\right) \tag{5}$$

$$L_{e10} = {}^{30}/_{2f_{10}\sqrt{\varepsilon_{re}}} \tag{6}$$

$$r = {}^{L_{e10}}/_{3.1} \tag{7}$$

$$\lambda_{10g} = {}^{30}/_{f_{10}\sqrt{\varepsilon_{re}}} \tag{8}$$

In the reconfigurable design of S-MSA that provides the tuning, the center frequency of AR BW is close to $TM_{30}$ mode frequency of the Sectoral patch. Initially, the resonant length formulation at $TM_{30}$ mode in 340° S-MSA is realized. For this, the surface current distribution at $TM_{30}$ mode is studied, and based on it formulation is obtained as given in Equations (9) and (10). In Equation (10), '$c$' equals 30. Using an FR4 substrate and for $r = 5.5$, $h_a = 2.3$, $h = 0.16$ cm, the calculated frequency is 1498 MHz, which is very close to the simulated frequency of 1510 MHz.

$$L_{e30} = 0.9r\left(\left({}^{340}/_{360}\right)2\pi\right) \tag{9}$$

$$f_{30} = {}^{3c}/_{2L_{e30}\sqrt{\varepsilon_{re}}} \tag{10}$$

Using the above formulation for 340° S-MSA, frequency reconfigurable design of S-MSA is realized to cover GPS L bands. In GPS L band, L5 (1176 MHz), L2 (1227 MHz), L3 (1381 MHz), and L1 (1575 MHz) bands exist. To completely cover the L-band, the frequency tuning of 399 MHz (25.33%), as calculated with respect to L1 band frequency, is needed. The proposed frequency reconfigurable S-MSA yields frequency tuning of 20.6%, and thus the entire L band cannot be addressed. Hence, the frequency reconfigurable design is presented to cover L5, L2, and L3 bands. For this, frequency tuning of 205 MHz (14.84%) is needed, which is offered by the proposed design. Initially, 340° S-MSA is designed for GPS L5 band. For this band, $f_{cAR} = f_{30} = 1176$ MHz. The substrate thickness at this frequency is calculated by using Equation (11). As the initial value of $h_a$ is not available, $\varepsilon_{re}$ is selected to be 1.045 in the initial calculation. Based on this, $h_t$ is obtained, and for FR4 substrate, $h_a$ is selected, which is an

**TABLE 2.** Results for reconfigurable S-MSA to cover GPS L5, L2 and L3 band.

| MSA | Simu. BW $S_{11} \leq -10$ dB (MHz, %) | Meas. BW $S_{11} \leq -10$ dB (MHz, %) | Simu. BW AR $< 3$ dB (MHz, %) | Meas. BW AR $\leq 3$ dB (MHz, %) | $f_{cAR}$ (MHz) | Peak Gain (dBic) |
|---|---|---|---|---|---|---|
| 340° S-MSA, L5 band | 236, 18.65 | 242, 19.05 | 32, 2.74 | 35, 2.9 | 1167 | 6.7 |
| 330° S-MSA, L2 band | 245, 19.1 | 256, 19.8 | 84, 6.9 | 90, 7.05 | 1216 | 6.0 |
| 300° S-MSA, L3 band | 317, 23.87 | 327, 24.02 | 141, 10.56 | 147, 10.92 | 1335 | 5.4 |

integer number. Using these substrate parameters, $\varepsilon_{re}$ is recalculated using Equation (3) at $TM_{30}$ mode. This value is retained in all further calculations. Resonant length at $TM_{30}$ mode and patch radius of 340° S-MSA is calculated using Equations (12) and (13), respectively. Equation (13) is obtained by rearranging the terms on two sides of Equation (9). Proximity strip parameters are selected as $h_s = 0.1062\lambda_{30g}$, $L_s = 0.055\lambda_{30g}$, $x_f = 0.1365\lambda_{30g}$. Here, $\lambda_{30g}$ is the wavelength at $TM_{30}$ mode, calculated using Equation (14).

$$h_t = 0.124\left({}^{30}/_{f_{30}\sqrt{\varepsilon_{re}}}\right) \tag{11}$$

$$L_{e30} = {}^{3c}/_{2f_{30}\sqrt{\varepsilon_{re}}} \tag{12}$$

$$r = {}^{L_{e30}}/_{5.34} \tag{13}$$

$$\lambda_{30g} = {}^{30}/_{f_{30}\sqrt{\varepsilon_{re}}} \tag{14}$$

Using this methodology, 340° S-MSA is designed for $f_{cAR} = 1176$ MHz, and calculated antenna dimensions are $h = 0.16$, $h_a = 2.9$, $r = 7.2$, $h_s = 2.65$, $x_f = 3.4$, $L_s = 1.4$ cm. This design achieves AR BW centered around 1177 MHz as per the requirements of L5 band. The L2 and L3 bands center frequencies are 1227 and 1381 MHz, respectively. To address these two frequency bands, 330° and 300° S-MSAs were simulated for the above mentioned antenna parameters. They yield AR BWs centered around 1230 and 1377 MHz. At all these bands, S-MSA offers AR BW that satisfactorily meets the requirements of each GPS L band for $S_{11} \leq -10$ dB. Based on this reconfigurable design is realized. In the reconfigurable design, 340°, 330°, and 300° S-MSAs are realized. With reference to Fig. 8(b), the design will be initiated with 300° S-MSA for radius $r = 7.2$ cm. By ensuring a gap of 0.1 cm, two circular sectors are placed in an empty area of 300° S-MSA. The circular sector placed in the immediate vicinity of 300° sectoral patch has angle $\theta_1 = 29$, and the circular sector next to it has an angle of 9. The radius of two circular sectors is selected as $r_2 = r_3 = 6.2$ cm. In reconfigurable design, the radius of parasitic sectors is selected in the range of 0.85–0.9 r. Here, depending upon the frequency application, minor parametric optimization for $r_2$ and $r_3$ is needed to achieve frequency tuning and AR BW as per the desired band. The connection of the first sector to 300° S-MSA through PIN diodes will realize 330° S-MSA, whereas electrical connection of second sector to this composite 330° S-MSA will realize 340° S-MSA. As shown in Fig. 8(b), four PIN diodes each is placed to inter-connect each sector to the initial 300° S-MSA. Thus as against the initial reconfigurable design shown in Fig. 8(b), for the S-MSA in GPS L band, two circular sectors along with 300° S-MSA are needed. This choice of sectoral angle and number of sectoral patches purely depends upon the application being targeted. The only upper limit comes with the maximum tuning of 20.6% possible with a reconfigurable S-MSA to achieve the broadside pattern and gain characteristics. For the above mentioned antenna parameters in the reconfigurable design, 300° S-MSA and circular sectors supported with the activation of PIN diodes are simulated, and their response is experimentally verified. Results for the reconfigurable designs are presented in Table 2. In all the designs, the center frequency of AR BW is near the desired L band frequency. Also, AR BW obtained in each case covers the exact L5, L2, and L3 band spectrums with their respective BW requirements. The peak antenna gain in all the configurations is more than 4.5 dBic, thus satisfying the requirements of each GPS L band. Therefore, using the proposed methodology, frequency reconfigurable tunable CP response is obtained in S-MSA for the given wireless application.

## 5. RESULTS DISCUSSION AND COMPARATIVE ANALYSIS

The CP design of 350° S-MSA offers AR BW of around 2% whereas varying angle reconfigurable S-MSA gives tunable CP response offering 20.6% of frequency tuning. Thus in terms of the range covered, reconfigurable design offers optimum performance. Hence to compare the novelty in the proposed configuration, it is compared against reported CP variations. The comparison is presented for measured $S_{11}$ & AR BW and peak gain against the antenna volume. As the configurations compared in Table 3 are designed over different frequencies and substrate parameters, the patch area and substrate thickness in all the designs are normalized with respect to wavelength at the center frequency of AR BW.

The e-slot cut design discussed in [3], multi-band design using slots and stubs presented in [4], and slot cut and shorted design for wider AR beam-width proposed in [5] offer lower AR BW as they employ thinner but efficient microwave substrate. While employing the shorting post, CP designs are reported in [6, 7], but they offer lower AR BW. Also considering the shorting post, which of the shorted patch resonant modes that contribute to the AR BW is not highlighted. Modified patch shape design using overlapped square patches [8] offers AR BW lower than 1%. The modified ring shape design discussed in [9] offers triple band response to cover GPS L5, L2, and L1 bands, but the antenna gain is lower than 4 dBi in the three bands. Further, the study presented in [9] does not discuss

**TABLE 3**. Comparison for the proposed frequency reconfigurable S-MSA against the reported CP configurations.

| MSA shown in | Meas. BW (MHz, %) | AR BW (MHz, %) | Peak Gain (dBi) | Area ($A_P/\lambda^2_{cAR}$) | Substrate thickness ($h_t/\lambda_{cAR}$) |
|---|---|---|---|---|---|
| Fig. 8(b), 340° S-MSA | 323, 21.98 | 72, 5.14 (20.6% frequency tuning) | 8.0 | 0.210 | 0.119 |
| Ref [3] | 75, 3.15 | 40, 1.673 | 5 | 0.892 | 0.02 |
| Ref [4] | 121, 4.99 | 13, 0.53 | 7.5 | 1.512 | 0.01 |
| Ref [5] | 27, 1.71 | 10, 0.63 | 5.4 | 0.14 | 0.03 |
| Ref [6] | 67, 2.72 | 16, 0.653 | 7.6 | 0.51 | 0.04 |
| Ref [7] | 350, 6.8 | 34, 1.33 | 10.3 | 0.241 | 0.04 |
| Ref [8] | 35, 2.2 | 8, 0.5 | 3.9 | .05 | 0.02 |
| Ref [9] | — | 46, 3.9 | 3.45 | 0.41 | 0.01 |
| Ref [10] | 3600, 62.94 | 3160, 53.92 | 3.6 | 0.457 | 0.035 |
| Ref [11] | 260, 11.2 | 90, 3.9 | 9.0 | 0.12 | 0.077 |
| Ref [12] | 230, 9.27 | 230, 9.27 | 8.3 | 0.19 | 0.08 |
| Ref [14] | 810, 35 | 130, 5.3 | 9.0 | 0.21 | 0.1 |
| Ref [15] | 710, 29.64 | 480, 20.08 | 11.5 | >2.5 | 0.095 |
| Ref [16] | 162, 5.71 | 60, 2.14 | 5.5 | 0.233 | 0.02 |
| Ref [18] | 30, 1.9 | 6, 0.4 | 2.3 | 0.215 | 0.05 |
| Ref [19] | 109, 4.52 | 26, 1.08 | 4.62 | 1.035 | 0.026 |
| Ref [20] | 180, 6 | 100, 3.3 | 2.7 | 0.82 | 0.03 |
| Ref [21] | 300, 15.2 | 160, 8.2 | 7.0 | 0.14 | 0.067 |
| Ref [22] | 80, 4.1 | 30, 1.54 | 8.4 | 2.362 | 0.05 |
| Ref [23] | 4200, 82 | 4100, 80 | 6.7 | 0.367 | 0.338 |
| Ref [24] | 2000, 40 | 1000, 19 | 7.5 | 0.65 | 0.12 |
| Ref [25] | 1570, 28.11 | 1160, 21.05 | 8.0 | 0.15 | 0.183 |
| Ref [26] | 330, 9.36 | 250, 7.13 | 7.75 | 0.67 | 0.052 |
| Ref [27] | 3080, 63.3 | 3040, 63.7 | 17.77 | 6.2 | 0.101 |
| Ref [28] | 1203, 49.29 | 488, 20.11 | 7.5 | 0.32 | 0.14 |

the design methodology to realize similar modified ring shape configuration as per any other frequency bands. Modified patch shape design discussed in [10] offers large AR BW, but antenna gain is lower. In addition, details about antenna functioning in terms of patch resonant modes, which contribute to the AR BW, and design methodology are not presented. Resonant slot cut designs are the optimum configurations to achieve CP response using a single patch [11–15]. However, they do not offer tuning in the center frequency of AR BW. Modified ground plane configurations employ thinner efficient microwave substrate to achieve CP response [16–19]. This substrate increases the antenna cost, while modified ground plane increases the back-lobe radiation that affects the gain. Further, they do not offer any frequency tuning as offered by the proposed S-MSAs. While adding parasitic half wavelength or quarter wavelength resonators in the planar or stacked layer, AR BW greater than 10% is not achieved [20–22]. The co-planar waveguide fed design discussed in [23] offers substantially large AR BW, but due to a backing reflecting sheet, overall antenna size is very large. The multiple slots loaded design discussed in [24] does not offer CP characteristics in the broadside direction, whereas wider U-slot loaded design discussed in [25] requires large substrate thickness. Also in [25], the additional U-slot cut patch mode that offers increment in the AR BW against the earlier reported U-slot cut CP design is not mentioned. Orthogonally coupled multiple patch design discussed in [26] offers AR BW lesser than 10%, whereas gap-coupled and stacked CP array design discussed in [27] requires large antenna volume. Gap-coupled CP design discussed in [28] offers AR BW of 20%, but the antenna size is higher. The reconfigurable MSA discussed in [29] offers switching between the dual or triple frequency responses. However, frequency tuning to scan particular wireless application is not possible there. Multiple stubs loaded design discussed in [30] suffers from the variation in broadside gain by 5–6 dBi, over the AR BW. U-slot loaded reconfigurable design discussed in [32] only offers switching between the broadside and end-fire radiation characteristics, whereas reconfigurable modified patch shape design discussed in [33] yields dual band dual sense CP response, without any frequency tuning.

Against the reported CP designs, proposed reconfigurable S-MSA offers a single patch solution that achieves tuning in the center frequency of AR BW and scans a frequency band of nearly 20%. To achieve this, a slot/stub, modified patch shape, is not used, but patch sectoral angle is varied that achieves the

tuning in the frequency of $TM_{30}$ resonant mode. The orthogonal surface current contribution at $TM_{30}$ mode achieves the CP response. With a 20% of tuning range achieved in the proposed design, it can cater to many of the wireless applications, e.g., a design for GPS L band application, as discussed above. Over the complete reconfigurable sectoral angle range, the gain of larger than 5 dBic is achieved, which is an appreciably large value from the practical application. Thus, a single patch CP design, which offers tuning in the center frequency of AR BW by 20% while changing sectoral angle, and without using additional slot/stub or parasitic patches, is the new contribution in the proposed work.

Measurements of the fabricated prototype were carried out inside the antenna laboratory, due to which variations/uncertainty in the measured antenna parameter exists. Since the measurement is not conducted inside an anechoic chamber, exact duplication of the radiation pattern plots as observed in the simulation is not obtained in the measurement. The deviation is observed in the shape of the pattern plots, especially the back-lobe radiation. However, the nature of the pattern plots remains the same in two cases, thus giving a good agreement. The air suspended configurations employing thicker substrate are used, and thus antenna parameters variation subject to substrate parameters is absent. However, variations in the bandwidth values and their frequencies are observed due to the variations in the exact value of the air gap maintained for patch and proximity strip. Small variation of the measured gain curve from the simulated gain curve arises due to the alignment problems of the two antennas along the vertical and horizontal axis of the measurement, in the three-antenna method. However, considering all these, good agreement between the measured and simulated data is achieved.

## 6. CONCLUSIONS

Reconfigurable designs of S-MSA to achieve CP response at sectoral patch $TM_{10}$ and $TM_{30}$ modes is proposed. For the design at $TM_{10}$ mode, 350° S-MSA offers optimum performance. On conventional ground plane, CP design offers 2.5% of AR BW that lies inside $S_{11}$ BW of more than 40%. Its wideband counterpart offers $S_{11}$ BW of more than 30%. The H-shape ground plane design backing the reconfigurable 350° S-MSA is proposed. The modified ground plane technique achieves reduction in the substrate thickness by $0.012\lambda_{cAR}$ and achieves a CP response using smaller sized ground plane. The reconfigurable design of S-MSA operating at $TM_{30}$ mode against the variation in sectoral angle is presented. The variation in angle alters the frequency of $TM_{30}$ mode and achieves the tuning in the center frequency of CP BW. Variation in sectoral angle by 60° achieves AR BW center frequency tuning by 20.6%. This tuning range helps to cover many of the adjoining wireless applications, thus providing a single antenna solution. Proposed reconfigurable design offers a broadside radiation pattern with a gain of more than 5 dBic over a complete range. A design methodology is presented for 350° and varying sectoral angle S-MSA. This helps to design similar configurations as per specific frequency application.

## REFERENCES


[1] Kumar, G. and K. P. Ray, *Broadband Microstrip Antennas*, Artech House, 2002.

[2] Wong, K.-L., *Compact and Broadband Microstrip Antennas*, John Wiley & Sons, 2004.

[3] Bernard, L. B. K., Nasimuddin, and A. Alphones, "AN e-shaped slotted-circular-patch antenna for circularly polarized radiation and radiofrequency energy harvesting," *Microwave and Optical Technology Letters*, Vol. 58, No. 4, 868–875, 2016.

[4] Tan, Q. and F.-C. Chen, "Triband circularly polarized antenna using a single patch," *IEEE Antennas and Wireless Propagation Letters*, Vol. 19, No. 12, 2013–2017, 2020.

[5] Wang, M.-S., X.-Q. Zhu, Y.-X. Guo, and W. Wu, "Compact circularly polarized patch antenna with wide axial-ratio beamwidth," *IEEE Antennas and Wireless Propagation Letters*, Vol. 17, No. 4, 714–718, 2018.

[6] Zhang, X., L. Zhu, and N.-W. Liu, "Pin-loaded circularly-polarized patch antennas with wide 3-dB axial ratio beamwidth," *IEEE Transactions on Antennas and Propagation*, Vol. 65, No. 2, 521–528, 2017.

[7] Zhang, X. and L. Zhu, "High-gain circularly polarized microstrip patch antenna with loading of shorting pins," *IEEE Transactions on Antennas and Propagation*, Vol. 64, No. 6, 2172–2178, 2016.

[8] Shi, Y. and J. Liu, "A circularly polarized octagon-star-shaped microstrip patch antenna with conical radiation pattern," *IEEE Transactions on Antennas and Propagation*, Vol. 66, No. 4, 2073–2078, 2018.

[9] Agrawal, N., A. K. Gautam, and R. Mishra, "Design of low volume circularly polarized annular ring-shaped planar antenna for gps applications," *International Journal of RF and Microwave Computer-Aided Engineering*, Vol. 31, No. 7, e22698, 2021.

[10] Midya, M., S. Bhattacharjee, and M. Mitra, "Broadband circularly polarized planar monopole antenna with G-shaped parasitic strip," *IEEE Antennas and Wireless Propagation Letters*, Vol. 18, No. 4, 581–585, 2019.

[11] Lee, K. F., K. M. Luk, W. C. Mok, and P. Nayeri, "Single probe-fed circularly polarized patch antennas with U-slots," *Microwave and Optical Technology Letters*, Vol. 53, No. 6, 1245–1253, 2011.

[12] Khidre, A., K. F. Lee, F. Yang, and A. Elsherbeni, "Wideband circularly polarized E-shaped patch antenna for wireless applications [wireless corner]," *IEEE Antennas and Propagation Magazine*, Vol. 52, No. 5, 219–229, 2010.

[13] Chen, Y. and C.-F. Wang, "Characteristic-mode-based improvement of circularly polarized U-slot and E-shaped patch antennas," *IEEE Antennas and Wireless Propagation Letters*, Vol. 11, 1474–1477, 2012.

[14] Kovitz, J. M., H. Rajagopalan, and Y. Rahmat-Samii, "Circularly polarised half E-shaped patch antenna: A compact and fabrication-friendly design," *IET Microwaves, Antennas & Propagation*, Vol. 10, No. 9, 932–938, 2016.

[15] Kovitz, J. M., H. Rajagopalan, and Y. Rahmat-Samii, "Design and implementation of broadband MEMS RHCP/LHCP reconfigurable arrays using rotated E-shaped patch elements," *IEEE Transactions on Antennas and Propagation*, Vol. 63, No. 6, 2497–2507, 2015.

[16] Ambekar, A. G. and A. A. Deshmukh, "Low profile design of regular shape microstrip antennas backed by fractal slots cut ground plane for circular polarized response," *Progress In Electromagnetics Research C*, Vol. 129, 203–219, 2023.

[17] Wei, K., B. Zhu, and M. Tao, "The circular polarization diversity antennas achieved by a fractal defected ground structure," *IEEE*

*Access*, Vol. 7, 92 030–92 036, 2019.

[18] Wei, K., J. Y. Li, L. Wang, R. Xu, and Z. J. Xing, "A new technique to design circularly polarized microstrip antenna by fractal defected ground structure," *IEEE Transactions on Antennas and Propagation*, Vol. 65, No. 7, 3721–3725, 2017.

[19] Pandey, S. K., G. P. Pandey, and P. M. Sarun, "Circularly polarized micro-strip antenna with fractal trees loaded ground plane," *Electromagnetics*, Vol. 39, No. 7, 505–523, 2019.

[20] Lin, J.-F. and Q.-X. Chu, "Enhancing bandwidth of CP microstrip antenna by using parasitic patches in annular sector shapes to control electric field components," *IEEE Antennas and Wireless Propagation Letters*, Vol. 17, No. 5, 924–927, May 2018.

[21] Cheng, G., B. Huang, Z. Huang, and L. Yang, "A high-gain circularly polarized filtering stacked patch antenna," *IEEE Antennas and Wireless Propagation Letters*, Vol. 22, No. 5, 995–999, 2023.

[22] Chen, J., C. Jin, B. Zhang, and Z. Shen, "Combined triangle quarter-wavelength patches and their application to high-gain CP antenna," *IEEE Antennas and Wireless Propagation Letters*, Vol. 19, No. 1, 104–108, Jan. 2019.

[23] Ullah, U., S. Koziel, and I. B. Mabrouk, "A simple-topology compact broadband circularly polarized antenna with unidirectional radiation pattern," *IEEE Antennas and Wireless Propagation Letters*, Vol. 18, No. 12, 2612–2616, Dec. 2019.

[24] Mondal, T., S. Maity, R. Ghatak, and S. R. B. Chaudhuri, "Design and analysis of a wideband circularly polarised perturbed psi-shaped antenna," *IET Microwaves, Antennas & Propagation*, Vol. 12, No. 9, 1582–1586, 2018.

[25] Zeng, J., X. Liang, L. He, F. Guan, F. H. Lin, and J. Zi, "Single-fed triple-mode wideband circularly polarized microstrip antennas using characteristic mode analysis," *IEEE Transactions on Antennas and Propagation*, Vol. 70, No. 2, 846–855, Feb. 2022.

[26] Wu, Q.-S., X.-Y. Tang, X. Zhang, L. Zhu, G. Zhang, and C.-B. Guo, "Circularly-polarized patch antennas with enhanced bandwidth based on capacitively coupled orthogonal patch radiators," *IEEE Open Journal of Antennas and Propagation*, Vol. 4, 472–483, 2023.

[27] Verma, A., M. Arrawatia, and G. Kumar, "High gain wideband circularly polarized microstrip antenna array," *IEEE Transactions on Antennas and Propagation*, Vol. 70, No. 11, 11 183–11 187, 2022.

[28] Deshmukh, A. A., V. A. P. Chavali, and A. G. Ambekar, "Circularly polarized gap-coupled designs of modified square microstrip antennas for WLAN and bluetooth applications," *Progress In Electromagnetics Research C*, Vol. 138, 233–246, 2023.

[29] Fakharian, M., P. Rezaei, and A. Orouji, "Reconfigurable multiband extended U-slot antenna with switchable polarization for wireless applications," *IEEE Antennas and Propagation Magazine*, Vol. 57, No. 2, 194–202, 2015.

[30] Nguyen-Trong, N., L. Hall, and C. Fumeaux, "A frequency- and polarization-reconfigurable stub-loaded microstrip patch antenna," *IEEE Transactions on Antennas and Propagation*, Vol. 63, No. 11, 5235–5240, 2015.

[31] CST Software Version 2019.

[32] Qin, P.-Y., Y. J. Guo, A. R. Weily, and C.-H. Liang, "A pattern reconfigurable U-slot antenna and its applications in MIMO systems," *IEEE Transactions on Antennas and Propagation*, Vol. 60, No. 2, 516–528, 2012.

[33] Kumar, P., S. Dwari, R. K. Saini, and M. K. Mandal, "Dual-band dual-sense polarization reconfigurable circularly polarized antenna," *IEEE Antennas and Wireless Propagation Letters*, Vol. 18, No. 1, 64–68, 2019.

[34] Toh, B. Y., R. Cahill, and V. F. Fusco, "Understanding and measuring circular polarization," *IEEE Transactions on Education*, Vol. 46, No. 3, 313–318, Aug. 2003.

[35] Deshmukh, A. A. and N. V. Phatak, "Broadband sectoral microstrip antennas," *IEEE Antennas and Wireless Propagation Letters*, Vol. 14, 727–730, 2014.

[36] Wu, Z.-F., W.-J. Lu, J. Yu, and L. Zhu, "Wideband null frequency scanning circular sector patch antenna under triple resonance," *IEEE Transactions on Antennas and Propagation*, Vol. 68, No. 11, 7266–7274, 2020.

[37] Yu, J., W.-J. Lu, Y. Cheng, and L. Zhu, "Tilted circularly polarized beam microstrip antenna with miniaturized circular sector patch under wideband dual-mode resonance," *IEEE Transactions on Antennas and Propagation*, Vol. 68, No. 9, 6580–6590, 2020.

[38] Chavali, V. A. P. and A. A. Deshmukh, "Wideband designs of regular shape microstrip antennas using modified ground plane," *Progress In Electromagnetics Research C*, Vol. 117, 203–219, 2021.